

Article

Slot-Loaded Microstrip Patch Sensor Antenna for High-Sensitivity Permittivity Characterization

Junho Yeo ^{1,*}  and Jong-Ig Lee ²

¹ School of Computer and Communication Engineering, Daegu University, 201 Daegudae-ro, Gyeongsan, Gyeongbuk 38453, Korea

² Department of Electronics Engineering, Dongseo University, 47 Jurye-ro, Sasang-gu, Busan 47011, Korea; leeji@dongseo.ac.kr

* Correspondence: jyeo@daegu.ac.kr; Tel.: +82-53-850-6642

Received: 2 April 2019; Accepted: 30 April 2019; Published: 7 May 2019



Abstract: A slot-loaded microstrip patch sensor antenna is proposed to enhance sensitivity in measuring the permittivity of planar materials. A thin rectangular slot was etched along the radiating edge of a rectangular patch antenna fed by a microstrip transmission line. Two resonant frequencies were created at a lower frequency compared to the single resonant frequency of a conventional ordinary patch antenna. The sensitivity of the proposed slot-loaded patch antenna was measured by the shift in the resonant frequency of the input reflection coefficient when the planar dielectric superstrate was placed above the patch, and was compared with that of a conventional patch antenna without the slot. The two antennas were designed and fabricated on a 0.76 mm-thick RF-35 substrate for the first resonant frequency to resonate at 2.5 GHz under unloaded conditions. Five different standard dielectric samples with dielectric constants ranging from 2.17 to 10.2 were tested for sensitivity comparison. The experiment results showed that the measured sensitivity of the proposed patch antenna were 3.54 to 4.53 times higher, compared to a conventional patch antenna, for the five samples.

Keywords: Slot-loaded microstrip patch sensor; high-sensitivity; radiating edge; permittivity characterization

1. Introduction

With rapid development of microwave technology, the frequency spectrum used by wireless systems has been considered up to the terahertz frequency band with sub-millimeter wavelengths, and accurate measurement of the permittivity of a material becomes more important for the design of antennas, microwave circuits, and non-destructive monitoring applications [1]. Among various permittivity measurement methods, those with planar resonators, such as split ring resonator (SRR) and complementary SRR (CSRR) structures, have been widely used because of their simple geometry, small size, ease of fabrication, and low cost [2–4]. In these methods, the material under test (MUT) is considered part of the resonator, and the permittivity can be deduced from the shift in resonant frequency.

Among the different planar structures, a microstrip structure consisting of a strip conductor and a ground plane separated by a dielectric substrate has been popular for permittivity measurement. Microstrip ring or open-loop resonators have been used to measure the dielectric constant of thin wafers, liquid solvents, or glucose–water solutions [5,6]. SRR- and CSRR-based sensors in the microstrip transmission line have been extensively studied for permittivity measurement [7–18]. Recently, a microstrip resonant sensor with an interdigital capacitor-based SRR structure was proposed in order to provide enhanced sensitivity for the characterization of dielectric materials at 2.45 GHz [19]. In addition, a high-sensitivity CSRR-based microstrip sensor based on an interdigital-capacitor-shaped

defected ground structure was proposed at 1.5 GHz under unloaded conditions, and its sensitivity was compared with conventional sensors based on a double-ring CSRR, a single-ring CSRR, and a rotated single-ring CSRR [20]. It turned out that the measured sensitivity of the proposed sensor was two times higher for a low-permittivity MUT at 2.17 and it was 1.42 times higher for a high-permittivity MUT at 10.2, when compared with the double-ring CSRR-based sensor.

Since a microstrip patch antenna can be considered a resonator, it has also been studied as a sensor for permittivity measurement of solid or liquid materials. A method to predict the resonant frequency of a microstrip patch antenna covered with a dielectric layer was proposed by using the effective dielectric constant of the whole structure, which can be calculated by using the variational technique [21]. Possible applications for this method were suggested to predict the detuning in the resonant frequency when the microstrip antenna is coated with protective layers, or subjected to icing conditions, or if it comes into contact with plasma. The resonant frequency and input impedance characteristics of probe-fed, rectangular, ordinary, and stacked microstrip patch antennas was presented for dielectric measurement when the antennas were loaded with a dielectric material [22]. The application of an air-spaced coaxial-fed rectangular microstrip patch antenna as a sensor was introduced for permittivity measurement of solid and liquid materials [23,24]. For planar solid materials, a sensor model based on a microstrip antenna with the MUT as a superstrate was derived. The effective dielectric constant of the superstrate-loaded microstrip antenna was calculated by using the filling factors of the substrate and superstrate. For liquid materials, the microstrip patch is considered to be buried in the liquid MUT, and an effective dielectric constant was derived by using that in the buried microstrip structure. Polytetrafluoroethylene, Thordon, nylon, and acrylic were used for solid-material measurements, whereas cyclohexane, pentanol, butan-1-ol, ethanol, and water were used for liquid-material measurements. Single- and dual-resonant microstrip patch antenna sensors were proposed for measuring moisture content ranging from 0% to 30% in peat and loam soil [25]. The shift in the resonant frequency of a microstrip patch antenna loaded with *Hevea* rubber latex at different levels of moisture content, ranging from 35% to 85%, was compared by using three different numerical methods [26]. A microstrip patch sensor antenna with a liquid chamber in the substrate was proposed for measuring the salinity in seawater [27]. A new method and prototype system for measuring the relative permittivity and loss tangent of dielectric materials has been developed by using a perturbation in the input impedance of a transmitting rectangular microstrip patch antenna when the MUT such as dielectric slab, disc or sphere is placed nearby the antenna with some spacing [28,29]. A new method to measure the complex conductivity of the graphene and thin film materials in a thin strip shape was proposed based on the reflection and transmission on the transverse electric (TE) modes in a rectangular waveguide [30]. A small portion of the MUT was placed inside the waveguide for permittivity characterization. However, the permittivity sensitivity of the microstrip patch antenna has not been systemically investigated in the literature, and an attempt to enhance the sensitivity of the microstrip patch antenna by modifying the resonant patch shape has not been tried.

In addition, various wireless interrogation mechanisms using passive antenna sensors without a battery have been investigated for sensing, such as temperature or strain. A radio frequency identification (RFID) sensor system consisting of a passive time-coded chip-less tag and a ultra wideband (UWB) reader has been developed [31]. The tag comprised an UWB slot antenna connected to a delay line loaded with a resistive temperature sensor. The tag was identified by changing the length of the delay line and the amplitude of the backscattered signals are modulated as a function of temperature in the range of 30–130 °C. A low-profile wireless passive temperature sensor using an open-ended cavity resonator/slot antenna has been demonstrated for harsh high-temperature applications up to 1000 °C [32]. The resonant frequency of the antenna sensor is determined by the temperature-dependent dielectric constant of alumina substrate. The temperature can be detected by sensing the resonant frequency of the sensor by using an open-ended waveguide interrogator antenna with a time-domain gating process. A real-time wireless vibratory strain sensing system consisting of a microstrip patch antenna strain sensor and a dynamic interrogator using a frequency modulated

continuous wave radar has been introduced [33]. The resonant frequency of the patch antenna varied as a function of the tensile strain it experiences. Far-field interrogation of a passive UWB microstrip patch antenna temperature sensor with a reactive impedance surface has been investigated [34]. The relationship between the normalized frequency shift of the antenna sensor and the temperature change up 280 °C was derived.

In this paper, we present a high-sensitivity microstrip patch sensor antenna based on a thin rectangular slot loaded along the radiation edge of the patch for permittivity measurement. The sensitivity of the proposed slot-loaded microstrip patch antenna was compared with a conventional patch antenna by measuring the shift in the resonant frequency of the input reflection coefficient when the planar dielectric superstrate was placed above the patch. The two antennas were designed and fabricated on a 0.76 mm-thick RF-35 substrate for the first resonant frequency to resonate at 2.5 GHz under unloaded conditions. Full-wave simulations were performed using CST Microwave Studio.

2. Slot-Loaded Microstrip Patch Sensor Design

Figure 1 shows the geometries of a conventional inset-fed rectangular microstrip patch antenna, a slot-loaded rectangular microstrip patch antenna, and a scaled slot-loaded rectangular microstrip patch antenna. The corresponding input reflection coefficient characteristics (S_{11}) of the three antennas are shown in Figure 2.

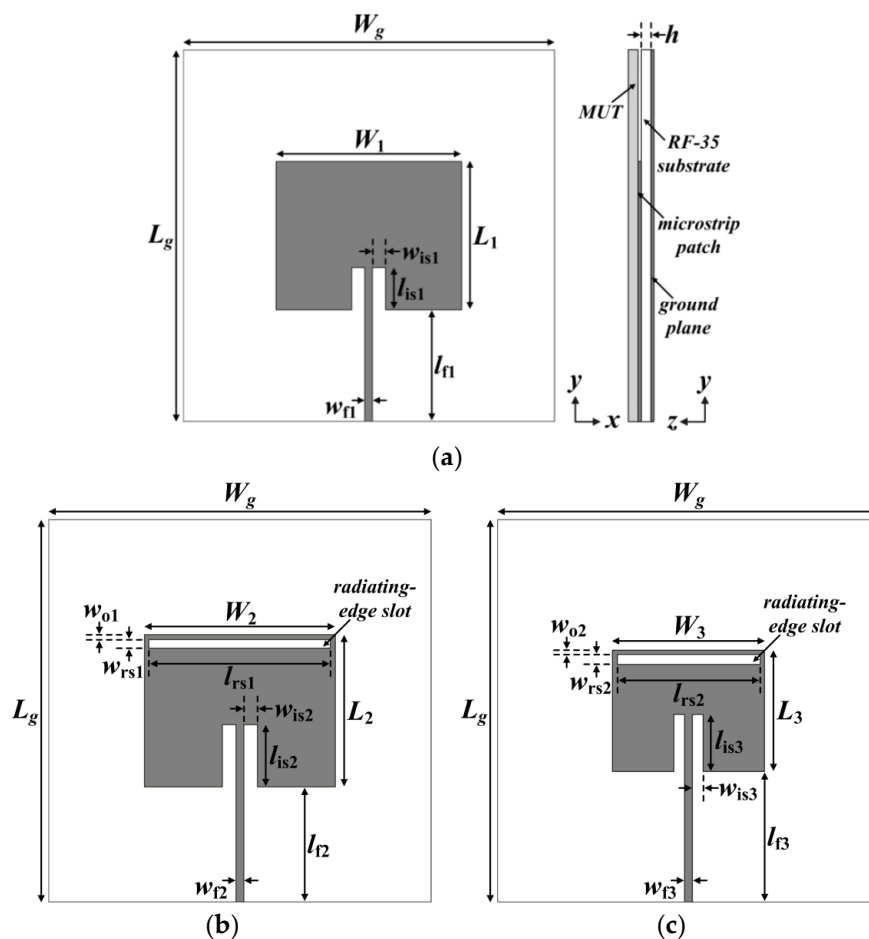


Figure 1. Geometries of microstrip patch sensor antennas: (a) Conventional inset-fed rectangular microstrip patch antenna; (b) slot-loaded rectangular microstrip patch antenna; (c) scaled slot-loaded rectangular microstrip patch antenna.

The conventional inset-fed rectangular microstrip patch antenna consisted of a rectangular patch with a 50-ohm microstrip feed line recessed inside the patch, and was printed on an RF-35 substrate ($\epsilon_r = 3.5$, $\tan \delta = 0.0018$, $h = 0.76$ mm), as shown in Figure 1a. The width and length of the 50-ohm microstrip feed line were $w_{f1} = 1.66$ mm and $l_{f1} = 24.5$ mm, respectively. The width and length of the rectangular patch were $W_1 = 40$ mm and $L_1 = 31.9$ mm, respectively, to resonate at 2.5 GHz, as shown in Figure 2. The width and length of the inset were $w_{is1} = 2.8$ mm and $l_{is1} = 9$ mm, respectively. The width and length of the ground plane were $W = L = 80$ mm. The MUT was placed above the patch as a superstrate for loaded conditions, as shown in Figure 2a. The width and length of the rectangular patch were calculated by using the following related equations [35]:

$$W = \frac{c}{2f_r} \sqrt{\frac{2}{\epsilon_r + 1}} \tag{1}$$

$$\epsilon_{reff} = \frac{\epsilon_r + 1}{2} + \frac{\epsilon_r - 1}{2} \left(1 + \frac{12h}{W}\right)^{-0.5} \tag{2}$$

$$\Delta L = 0.412h \frac{(\epsilon_{reff} + 0.3) \left(\frac{W}{h} + 0.264\right)}{(\epsilon_{reff} - 0.258) \left(\frac{W}{h} + 0.8\right)} \tag{3}$$

$$L = \frac{c}{2f_r \sqrt{\epsilon_{reff}}} - 2\Delta L \tag{4}$$

where W and L are the width and length of the rectangular patch, ϵ_r is the relative permittivity of the substrate, f_r is the resonant frequency, c is the speed of light in free space, ϵ_{reff} is the effective relative permittivity, h is the thickness of the substrate, and ΔL is the extension of the patch length due to the fringing effects.

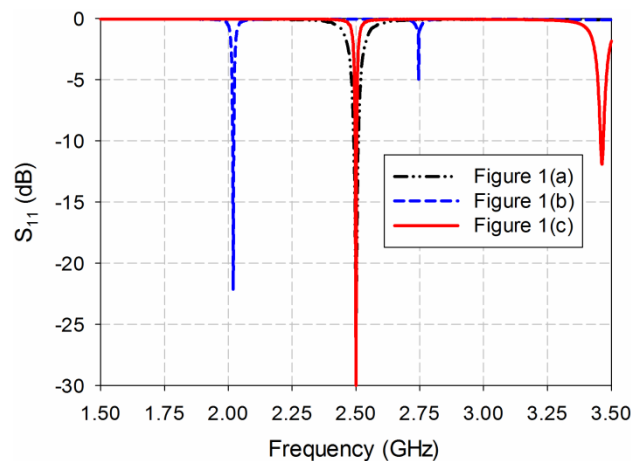


Figure 2. Input reflection coefficient characteristics (S_{11}) of the three antennas in Figure 1.

Next, a thin rectangular slot was etched along the radiating edge on the opposite side of the microstrip feed line in Figure 1a, as shown in Figure 1b. The widths and lengths of the patch, microstrip feed line, and ground plane were the same as those in Figure 1a: $W_2 = W_1$, $L_2 = L_1$, $w_{f2} = w_{f1}$, and $l_{f2} = l_{f1}$. The width and length of the thin rectangular slot were $w_{rs1} = 1$ mm and $l_{rs1} = 38$ mm, respectively. The distance between the radiating edge and the thin rectangular slot was $w_{o1} = 1$ mm. The width and length of the inset were $w_{is2} = 2.8$ mm and $l_{is2} = 13$ mm, respectively. It is well-known that dual resonant frequencies with similar radiating properties can be created when two narrow slots are inserted close to the radiating edges of the probe-fed patch [36]. In addition, since the electric field distributions of the microstrip patch antenna are maximal at the radiating edges, the permittivity sensitivity of the patch antenna might be improved by adding slots along the radiating

edges. When a thin rectangular slot was inserted along a radiating edge, two resonant frequencies were generated at $f_{r1} = 2.019$ GHz and $f_{r2} = 2.746$ GHz with a frequency ratio of $f_{r2}/f_{r1} = 1.36$, which is similar to the results in [36]. The variations in the two resonant frequencies for different slot widths w_{rs1} ranging from 1 mm to 5 mm are investigated in Figure 3. When w_{rs1} was increased to 3 mm, the first resonant frequency shifted to a lower frequency at $f_{r1} = 1.846$ GHz, whereas the second resonant frequency moved to a higher frequency at $f_{r2} = 2.858$ GHz. Therefore, the frequency ratio increased to $f_{r2}/f_{r1} = 1.55$. As w_{rs1} was further increased to 5 mm, the first resonant frequency moved further toward a lower frequency at $f_{r1} = 1.729$ GHz, whereas the second resonant frequency shifted further toward a higher frequency at $f_{r2} = 3.006$ GHz. The frequency ratio in this case becomes $f_{r2}/f_{r1} = 1.74$. Hence, the first resonant frequency moved toward a lower frequency, and the frequency ratio between the first and second resonant frequencies increased as slot width w_{rs1} increased.

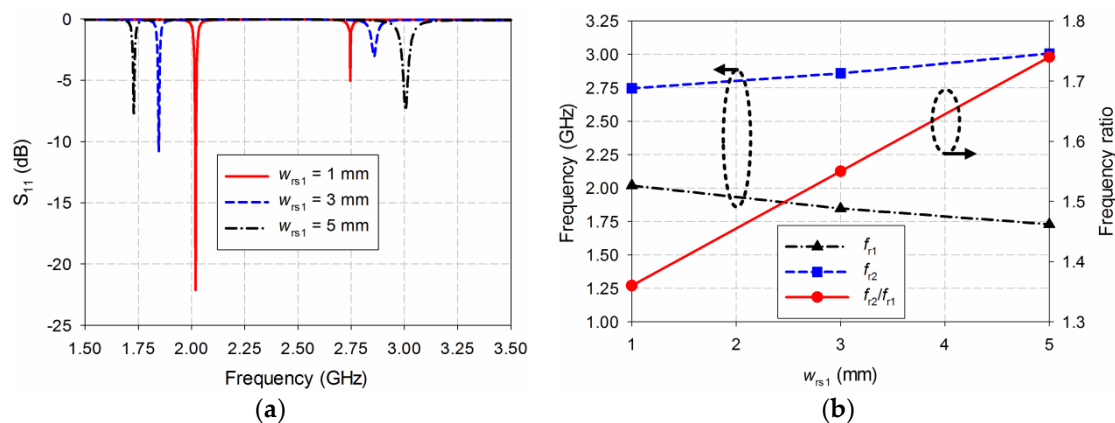


Figure 3. (a) S_{11} characteristics of the slot-loaded patch antenna in Figure 1b for varying slot widths w_{rs1} ; (b) the first and second resonant frequencies, and the frequency ratio vs. w_{rs1} .

Finally, the patch dimensions and slot length were scaled with a fixed slot width and distance of $w_{rs2} = w_{o2} = 1$ mm to have the first resonant frequency at 2.5 GHz to get the dielectric property at a common frequency compared to the conventional patch antenna in Figure 1a, because the permittivity of a material is dispersive as a function of frequency. The width of the microstrip feed line, and the widths and lengths of the ground plane were the same as those in Figure 1a ($w_{f3} = w_{f1}$). The width and length of the scaled slot-loaded patch were $W_3 = 31.8$ mm and $L_3 = 25.4$ mm, respectively, to resonate at 2.5 GHz, as shown in Figure 2. The patch dimensions were reduced about 20.4%, compared to those of the conventional patch antenna in Figure 1a. The slot length was decreased to $l_{rs2} = 29.8$ mm, whereas the length of the microstrip feed line was increased to $l_{f3} = 27.3$ mm. The width and length of the inset were $w_{is3} = 2.3$ mm and $l_{is3} = 12$ mm, respectively. The first resonant frequency was $f_{r1} = 2.5$ GHz, and the second was $f_{r2} = 3.465$ GHz, as shown in Figure 2. The frequency ratio in this case becomes $f_{r2}/f_{r1} = 1.39$, which was similar to that when the slot width was 1 mm. The frequency bandwidth of the first resonant frequency for a voltage standing wave ratio (VSWR) < 2 was 2.496–2.503 GHz, and its fractional bandwidth was 0.28%, which were quite reduced compared to the conventional patch antenna without slot loading (2.490–2.510 GHz, 0.8%) because of the size reduction of the slot-loaded patch. However, the quality factor at the first resonant frequency is increased to 357, compared to the conventional patch antenna (at 125). Figure 4 shows the electric field distributions of the conventional patch antenna and the proposed slot-loaded patch antenna. In the first resonant frequency of the proposed slot-loaded patch antenna, the electric-field distributions were more concentrated on the slot along the radiating edge, and this concentration area was more distributed compared to the first resonant frequency of the conventional patch antenna and the second resonant frequency of the slot-loaded patch antenna.

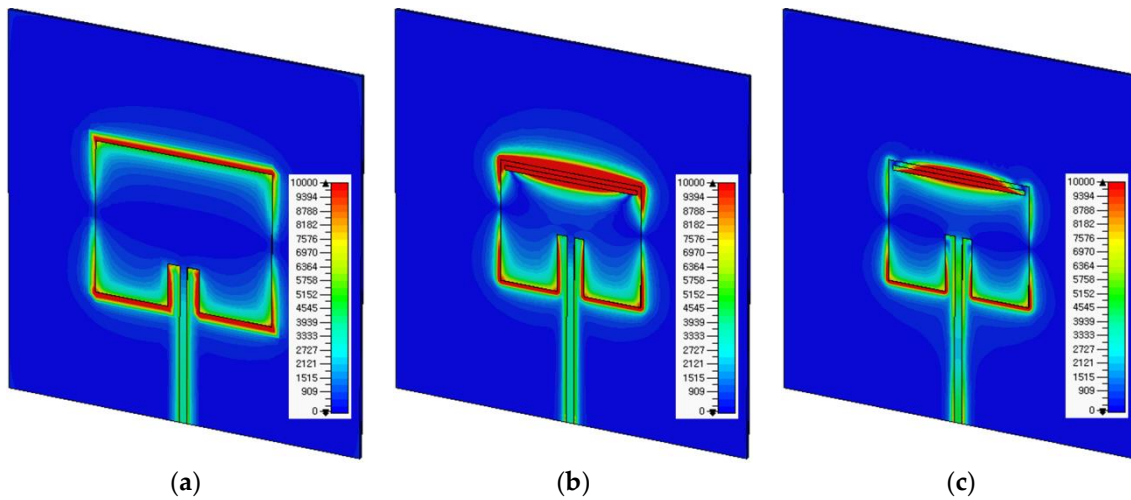


Figure 4. Electric field distributions of (a) conventional patch antenna at resonant frequency $f_{r1} = 2.5$ GHz; (b) proposed slot-loaded patch antenna at $f_{r1} = 2.5$ GHz; (c) proposed slot-loaded patch antenna at $f_{r2} = 3.465$ GHz.

3. Sensitivity Comparison

In this section, the sensitivity of the scaled slot-loaded microstrip patch antenna in Figure 1c is compared with the conventional patch antenna in Figure 1a by measuring the shift in the resonant frequency of the input reflection coefficient.

Figure 5 shows the S_{11} characteristics of the conventional patch antenna and the proposed slot-loaded patch antenna. The MUT was placed above the patch as a superstrate, and its relative permittivity (ϵ_r) was varied from 1 to 10 in steps of 1. In this case, the loss tangent of the MUT was set to 0 as in the lossless case. The width and length of the MUT were the same as those of the ground plane, and its thickness was chosen to be 1.6 mm because the thickest of the substrates available from Taconic Inc., which were used as the MUTs, is around 1.6 mm. For the conventional patch antenna, the first resonant frequency (f_{r1}) for S_{11} moved from 2.5 GHz to 2.312 GHz when ϵ_r increased from 1 to 10, whereas it shifted from 2.5 GHz to 1.854 GHz for the proposed patch antenna. In addition, the second resonant frequency (f_{r2}) of the proposed patch antenna moved from 3.466 GHz to 2.991 GHz when ϵ_r increased from 1 to 10. Table 1 summarizes the resonant frequencies of the S_{11} responses with a different relative permittivity of the MUT for the conventional and proposed patch antennas.

In order to compare the sensitivity performance of the proposed patch antenna with that of the conventional patch antenna, the shift in the resonant frequency (Δf_r), percent relative frequency shift (PRFS), enhancement in percent relative frequency shift (PRFSE), sensitivity (S), and sensitivity enhancement (SE) of S_{11} responses are defined as follows [3,12,13,37]:

$$\Delta f_r = f_{ru} - f_{rl} \text{ (GHz)} \tag{5}$$

$$PRFS = \frac{\Delta f_r}{f_r} = \frac{f_{ru} - f_{rl}}{f_{ru}} \times 100 \text{ (\%)} \tag{6}$$

$$PRFSE = \frac{PRFS_{proposed}}{PRFS_{conventional}} \tag{7}$$

$$S = \frac{\Delta f_r}{\Delta \epsilon_r} = \frac{f_{ru} - f_{rl}}{\epsilon_{ru} - \epsilon_{rl}} \tag{8}$$

$$SE = \frac{S_{proposed}}{S_{conventional}} \tag{9}$$

where Δf_r is the shift in the resonant frequency of the conventional and proposed patch antennas, f_{r1} is the resonant frequency of the conventional and proposed patch antennas for unloaded conditions, f_{r1} is the resonant frequency of the conventional and proposed patch antennas for loaded conditions, PRFS is the percent relative frequency shift of the resonant frequencies of the conventional and proposed patch antennas, PRFSE is the enhancement in the percent relative frequency shift of the first and second resonant frequencies of the proposed patch antenna compared to the conventional patch antenna, S is the sensitivity of the resonant frequencies of the conventional and proposed patch antennas with respect to the relative permittivity of the MUT, ϵ_{r1} is the relative permittivity of the MUT for unloaded conditions, ϵ_{r1} is the relative permittivity of the MUT for loaded conditions, and SE is the sensitivity enhancement of the first resonant frequency of the proposed patch antenna compared to the conventional patch antenna.

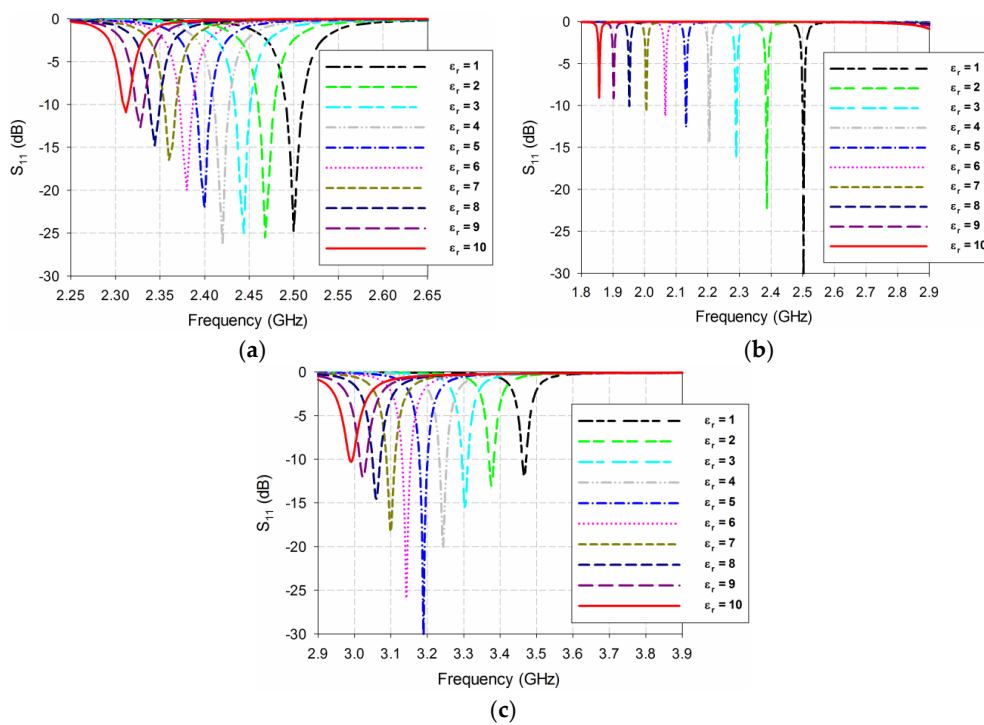


Figure 5. S_{11} characteristics of the conventional and proposed patch antennas when varying relative permittivity of the MUT: (a) Conventional f_{r1} ; (b) proposed f_{r1} ; (c) proposed f_{r2} .

Table 1. Resonant frequencies of S_{11} responses of the conventional and proposed patch antennas in GHz.

Antenna Type	Resonant Frequency	$\epsilon_r = 1$	$\epsilon_r = 2$	$\epsilon_r = 3$	$\epsilon_r = 4$	$\epsilon_r = 5$	$\epsilon_r = 6$	$\epsilon_r = 7$	$\epsilon_r = 8$	$\epsilon_r = 9$	$\epsilon_r = 10$
Conventional	f_{r1}	2.5	2.468	2.444	2.420	2.400	2.380	2.360	2.344	2.328	2.312
Proposed	f_{r1}	2.5	2.384	2.287	2.202	2.128	2.063	2.003	1.949	1.899	1.854
Proposed	f_{r2}	3.466	3.376	3.303	3.243	3.189	3.142	3.099	3.06	3.024	2.991

According to Equations (5)–(9), the sensitivity performance of the conventional and proposed patch antennas was analyzed from the results shown in Figure 5 and Table 1, and Δf_r of S_{11} for the conventional and proposed patch antennas is plotted in Figure 6a. Figure 6b shows the PRFS of the conventional and proposed patch antennas. The PRFSE for the first and second resonant frequencies of the proposed patch antenna, compared to that of the first resonant frequency of the conventional patch antenna, is presented in Figure 6c. Next, the S of the resonant frequencies of the conventional and proposed patch antennas is plotted in Figure 6d. Figure 6e presents the SE of the first resonant frequency of the proposed patch antenna compared to that of the conventional patch antenna. Note

that the S and SE of the second resonant frequency of the proposed patch antenna are not plotted and compared in Figure 6c,d because the second resonant frequency of the proposed patch antenna was different from the first resonant frequency of the conventional patch antenna, and their S and SE cannot be directly compared.

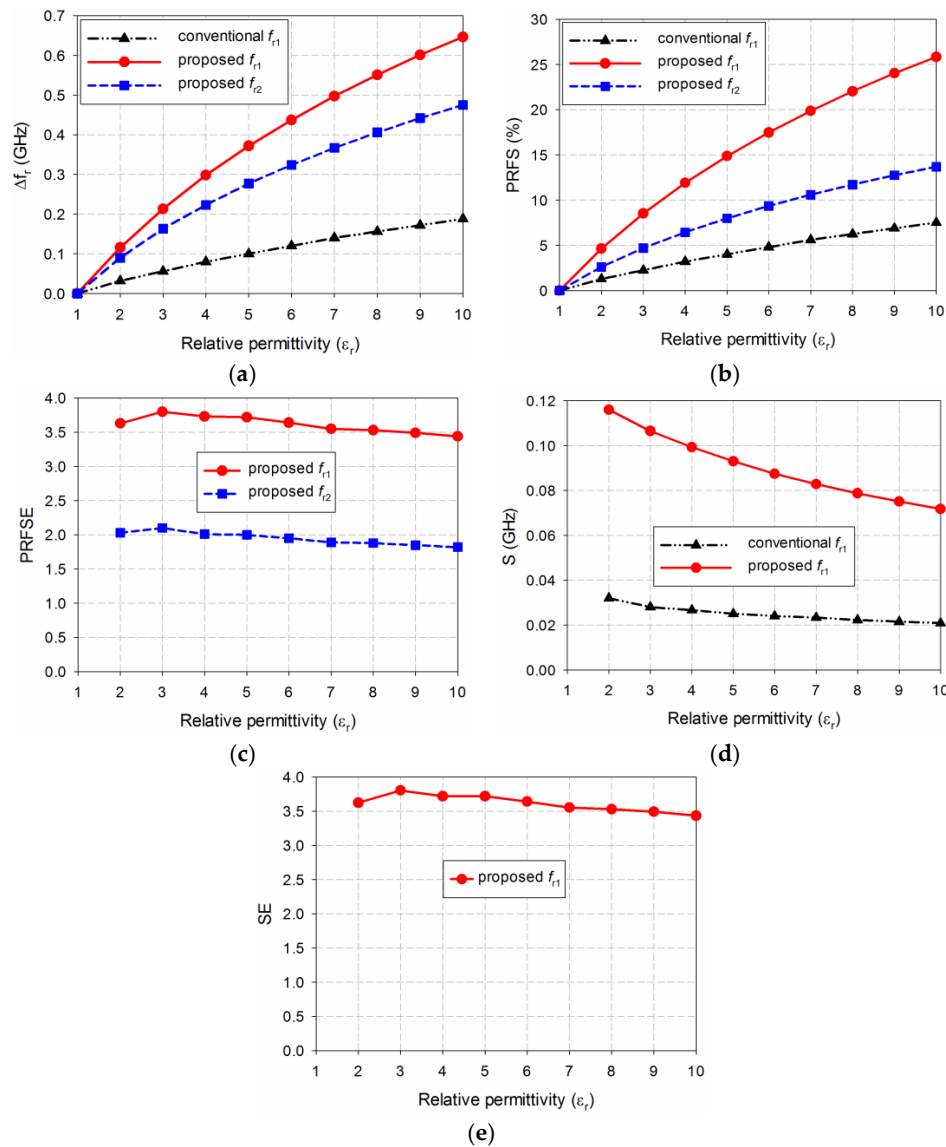


Figure 6. Sensitivity comparison of the conventional and proposed patch antennas: (a) Resonant frequency (Δf_r); (b) percentage relative frequency shift (PRFS); (c) enhancement in percent relative frequency shift (PRFSE); (d) sensitivity (S); (e) sensitivity enhancement (SE).

When the MUT was loaded above the patch, it affected the total capacitance and effective relative permittivity related to the microstrip patch resonator, and the S_{11} resonant frequency was a nonlinear function of the resonator related to the effective relative permittivity [23,24]. We observe from Figure 6d that sensitivity S was not constant as a function of relative permittivity, and it was higher for a smaller value of relative permittivity. For example, when the permittivity of the MUT was $\epsilon_r = 2$, frequency shift Δf_r in the first resonant frequency of the conventional patch antenna was 0.032 GHz, whereas the first and second resonant frequencies of the proposed patch antenna were 0.116 GHz and 0.09 GHz. The PRFS in the first resonant frequency of the conventional patch antenna was 1.28%, whereas the first and second resonant frequencies of the proposed patch antenna were 4.64% and 2.6%. Therefore, the PRFSE for the first and second resonant frequencies of the proposed patch antenna were 3.63 and

2.03. In this case, S was the same as Δf_r because the difference in the relative permittivity ($\Delta \epsilon_r$) was 1. SE of the first resonant frequency of the proposed patch antenna was 3.63. It is worthwhile to note that the PRFSE was the same as SE. Hence, SE for the second resonant frequency of the proposed patch antenna could be compared by using PRFSE.

When the permittivity of the MUT was increased to $\epsilon_r = 10$, frequency shift Δf_r in the first resonant frequency of the conventional patch antenna was 0.188 GHz, whereas the first and second resonant frequencies of the proposed patch antenna were 0.646 GHz and 0.475 GHz. PRFS in the first resonant frequency of the conventional patch antenna was 7.52%, whereas the first and second resonant frequencies of the proposed patch antenna were 25.84% and 13.7%. PRFSE for the first and second resonant frequencies of the proposed patch antenna were 3.44 and 1.82. The S of the first resonant frequency of the conventional and proposed patch antenna were 0.021 GHz and 0.072 GHz, respectively. SE of the first resonant frequency of the proposed patch antenna was 3.44. Hence, we can conclude that the sensitivity of the proposed patch antenna at the first resonant frequency was 3.44 to 3.63 times higher than the conventional patch antenna for relative permittivity ranging from 2 to 10.

Next, in order to investigate the effect of covering the feed line of the microstrip patch antenna with the MUT on the resonant frequency of the antenna, the S_{11} characteristics of the conventional and proposed patch antennas were compared when the length of the MUT was decreased from the input port of the antenna. For the conventional patch antenna, five different cases of the MUT length were simulated; 80 mm ($=L_g$, the MUT completely covered the feed line), 68 mm (the MUT covered half the feed line), 56 mm (the MUT covered the patch with the inset feed part), 47 mm (the MUT covered the patch without the inset feed part), 40 mm (the MUT covered half of the patch). The variations on the resonant frequency of the conventional patch antenna for five cases of varying the MUT length are plotted in Figure 7a. The PRFS of the resonant frequency of the conventional patch antenna is shown in Figure 8a. When the MUT length decreased from 80 mm to 68 mm, the shift in the resonant frequency was negligible, whereas the resonant frequency moved toward the high frequency linearly with an effect of sensitivity decrease when it further decreased to 56 mm and 47 mm. Note that the amount of the frequency shift increased as the relative permittivity of the MUT increased. For instance, when the permittivity of the MUT was $\epsilon_r = 2$, the PRFS in the first resonant frequency of the conventional patch antenna was 0.32% and 0.69% for the MUT length of 56 mm and 47 mm. When the permittivity of the MUT was increased to $\epsilon_r = 10$, the PRFS in the first resonant frequency of the proposed patch antenna was 2.34% and 4.37% for the MUT length of 56 mm and 47 mm.

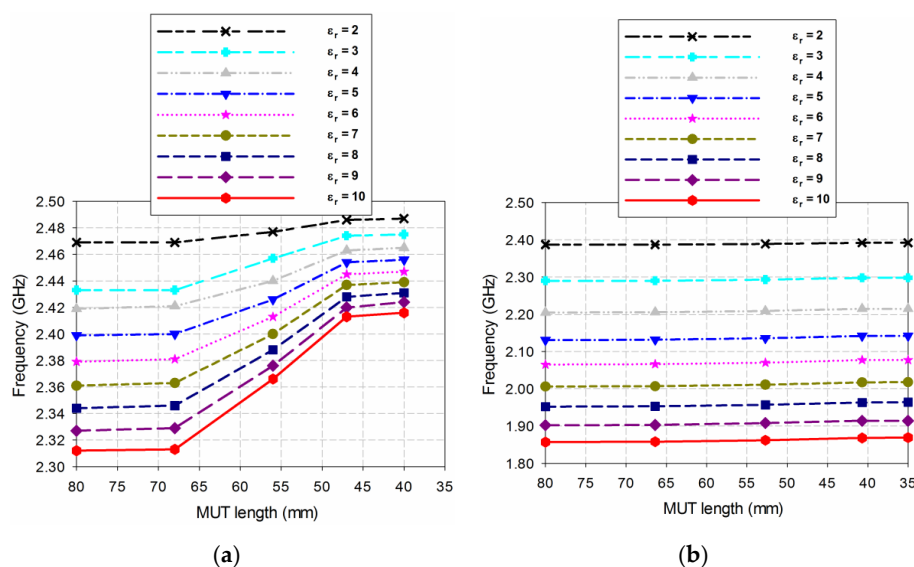


Figure 7. Variations on the resonant frequency of the conventional and proposed patch antennas when varying the length of the material under test (MUT): (a) Conventional f_{r1} ; (b) proposed f_{r1} .

For the proposed patch antenna, five different cases of the MUT length were also simulated; 80 mm ($=L_g$, the MUT covered completely the feed line), 66.4 mm (the MUT covered half the feed line), 52.7 mm (the MUT covered the patch with the inset feed part), 40.7 mm (the MUT covered the patch without the inset feed part), 35 mm (the MUT covered 30.3% of the patch). The variations on the resonant frequency of the proposed patch antenna for five cases of varying the MUT length are plotted in Figure 7b and the PRFS of the resonant frequency of the proposed patch antenna is shown in Figure 8a. When the MUT length decreased from 80 mm to 66.4 mm, the shift in the resonant frequency was negligible, whereas the resonant frequency moved toward the high frequency linearly when it further decreased to 52.7 mm and 40.7 mm. Note that the trend of the resonant frequency shift was similar to the conventional patch antenna, but the amount was relatively small. For example, when the permittivity of the MUT was $\epsilon_r = 2$, the PRFS in the first resonant frequency of the conventional patch antenna was 0.08% and 0.21% for the MUT length of 52.7 mm and 40.7 mm. When the permittivity of the MUT was increased to $\epsilon_r = 10$, the PRFS in the first resonant frequency of the proposed patch antenna was 0.27% and 0.59% for the MUT length of 52.7 mm and 40.7 mm.

The reason for this can be explained by the electric field distributions of the conventional and proposed patch antennas. For the conventional patch antenna, the electric fields were maxima at two radiating edges and, therefore, the covering region around both the two edges affected the resonant frequency of the antenna. However, for the proposed slot-loaded patch antenna, the electric fields were maxima nearby the loaded slot and the covering region nearby the slot would be enough. Hence, we can conclude that the proposed slot-loaded patch antenna had an advantage of relatively less effect on the MUT size for the resonant frequency shift and of using small size of the MUT compared to the conventional patch antenna.

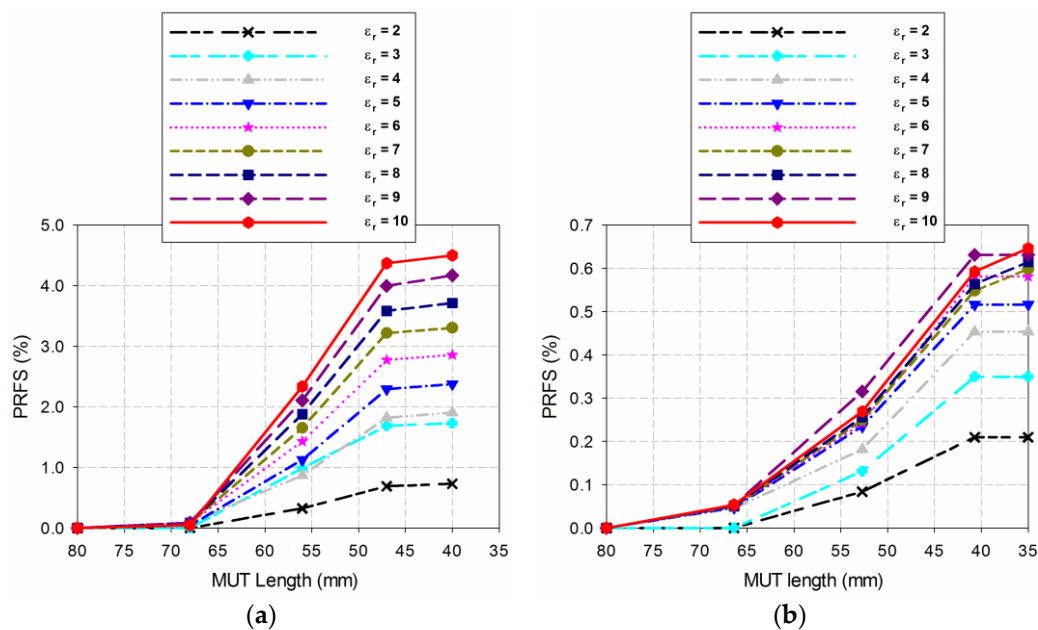


Figure 8. PRFS of the resonant frequency of the conventional and proposed patch antennas when varying the length of the MUT: (a) Conventional f_{r1} ; (b) proposed f_{r1} .

4. Experiment Results and Discussion

Prototypes of the conventional and proposed patch antennas described in the previous section were fabricated on an RF-35 substrate ($\epsilon_r = 3.5$, $\tan \delta = 0.0018$, $h = 0.76$ mm), as shown in Figure 9. The S_{11} characteristics of the fabricated antenna were measured using an Agilent N5230A network analyzer, and photographs of the experiment setup are shown in Figure 10. Five different standard dielectric MUTs from Taconic Inc. (Petersburgh, NY, USA). were tested for the sensitivity comparison.

The MUTs had relative permittivity ranging from 2.17 to 10.2, and their relative permittivity, loss tangent, and thickness from the data sheet in [38] are summarized in Table 2.

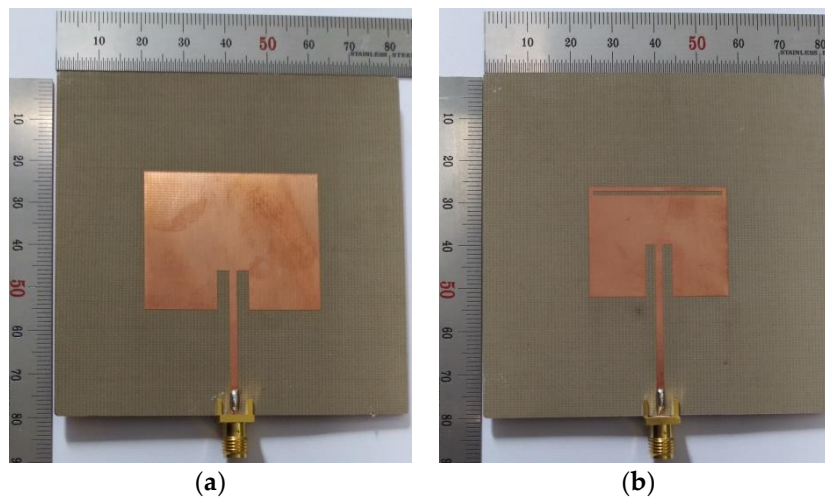


Figure 9. Photographs of the fabricated patch antennas: (a) Conventional; (b) proposed.

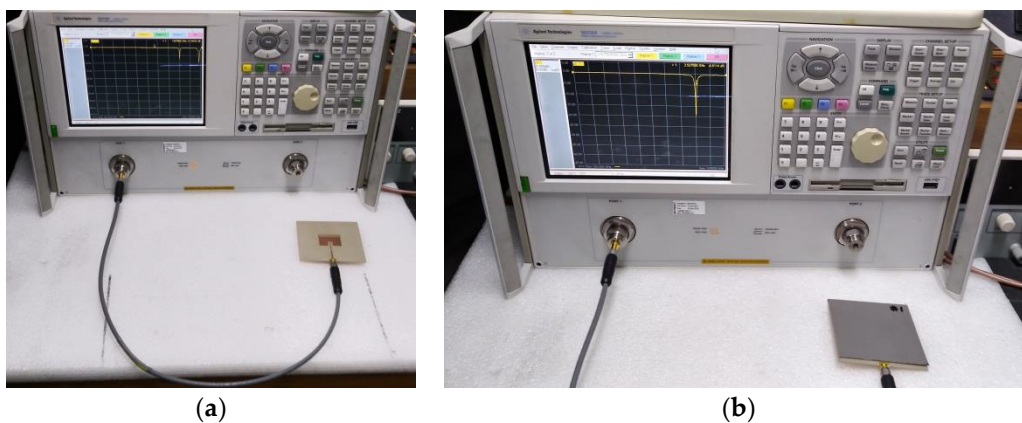


Figure 10. Experiment setups: (a) Unloaded; (b) loaded.

Table 2. Relative permittivity, loss tangent, and thickness of the five MUTs.

No.	MUT	ϵ_r	$\tan \delta$	Thickness
1	TLY-5A	2.17 ± 0.02	0.0009@10GHz	1.58 mm
2	RF-301	2.97 ± 0.07	0.0012@1.9GHz	1.52 mm
3	TRF-43	4.3 ± 0.15	0.0035@10GHz	1.63 mm
4	RF-60A	6.15 ± 0.15	0.0028@10GHz	1.52 mm
5	RF-10	10.2 ± 0.3	0.0025@10GHz	1.52 mm

The S_{11} characteristics of the conventional and proposed patch antennas were first simulated with the five MUTs in Table 2 placed above the patch, as shown in Figure 11. The length of the MUTs was slightly reduced to 75 mm because there is a protruding part in the subminiature version A (SMA) connector for soldering the input port of the fabricated antenna, as shown in Figure 10b. For the conventional patch antenna, the first resonant frequency for S_{11} moved from 2.465 GHz for the TLY-5A MUT ($\epsilon_r = 2.17$) to 2.312 GHz for the RF-10 MUT ($\epsilon_r = 10.2$). In the proposed patch antenna, the first resonant frequency shifted from 2.369 GHz for the TLY-5A to 1.852 GHz for the RF-10. Table 3 shows the first resonant frequencies of the simulated S_{11} responses for the conventional and proposed patch antennas.

Figure 12 compares the simulated sensitivity for the first resonant frequencies of the conventional and proposed patch antennas when the five MUTs are loaded. When TLY-5A ($\epsilon_r = 2.17$) was used as the MUT, the first resonant frequency shifts Δf_r of the conventional and proposed patch antennas were 0.035 GHz and 0.131 GHz, and the PRFS were 1.4% and 5.24%. The PRFSE for the first resonant frequency of the proposed patch antenna is 3.74. The S of the conventional and proposed patch antennas were 0.030 GHz and 0.112 GHz. The SE of the proposed patch antenna was 3.75. When RF-10 ($\epsilon_r = 10.2$) was used as the MUT, the first resonant frequency shifts Δf_r of the conventional and proposed patch antennas were 0.188 GHz and 0.648 GHz, respectively, and the PRFS were 7.52% and 25.92%. The PRFSE for the first resonant frequency of the proposed patch antenna was 3.45. The S in the conventional and proposed patch antennas were 0.020 GHz and 0.070 GHz, respectively. The SE of the proposed patch antenna was 3.45. Therefore, the trends in Δf_r , PRFS, PRFSE, S, and SE for the five MUTs were similar to those of the lossless case in Figure 6, and the only difference was the loss tangent. Since the loss tangent of the MUT influences the bandwidth or the quality factor of the S_{11} characteristics of the patch antennas [23,24], and the loss tangent of the MUTs is moderately low, ranging from 0.009 to 0.035, the effect of the low tangent on the S_{11} resonant frequencies would not be significant.

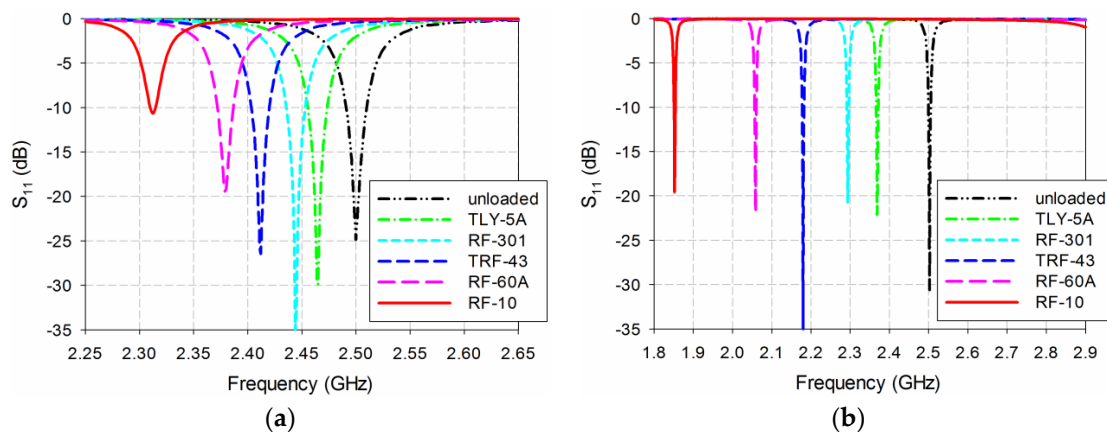


Figure 11. Simulated S_{11} characteristics of the conventional and proposed patch antennas for MUTs in Table 2: (a) Conventional; (b) proposed.

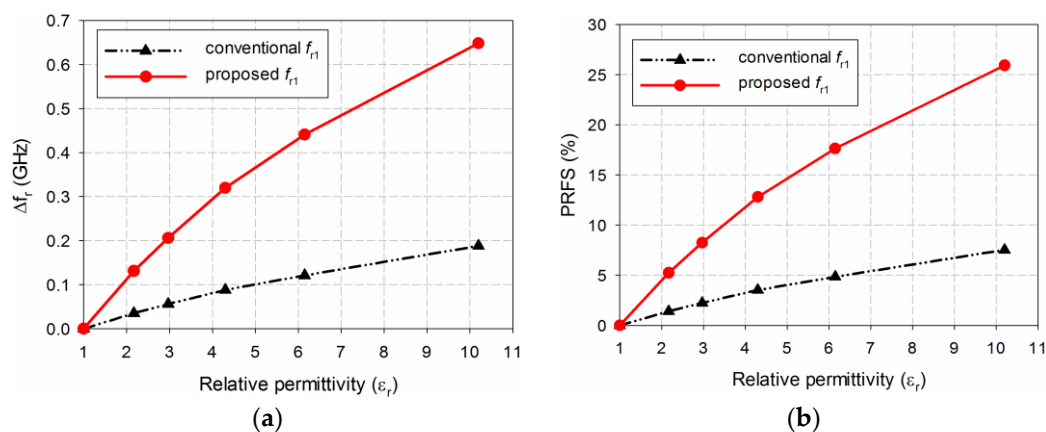


Figure 12. Cont.

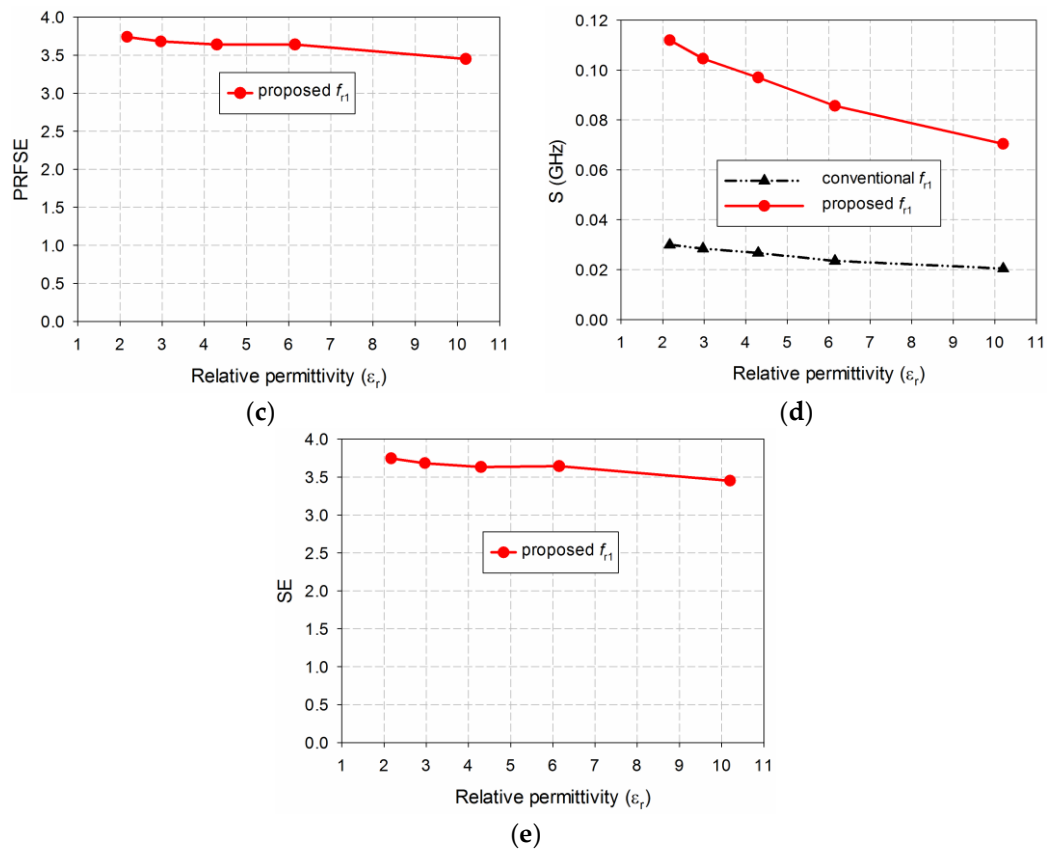


Figure 12. Simulated sensitivity comparison of the conventional and proposed patch antennas for the MUTs in Table 2: (a) Δf_r ; (b) PRFS; (c) PRFSE; (d) S; (e) SE.

Table 3. Simulated first resonant frequencies for S_{11} responses in the conventional and proposed patch antennas in GHz.

Antenna Type	Resonant Frequency	Unloaded ($\epsilon_r = 1$)	TLY-5A ($\epsilon_r = 2.17$)	RF-301 ($\epsilon_r = 2.97$)	TRF-43 ($\epsilon_r = 4.3$)	RF-60A ($\epsilon_r = 6.15$)	RF-10 ($\epsilon_r = 10.2$)
Conventional	f_{r1}	2.5	2.465	2.444	2.412	2.379	2.312
Proposed	f_{r1}	2.5	2.369	2.294	2.18	2.059	1.852

Next, the simulated sensitivity of the conventional and proposed patch antennas was validated by measuring their S_{11} characteristics when the five MUTs in Table 2 were placed above the patch, as shown in Figure 13. The length of the MUTs was slightly reduced to 75 mm. When unloaded, the first S_{11} resonant frequencies of the conventional and proposed patch antennas were 2.528 GHz and 2.508 GHz, respectively, which were close to the simulated resonant frequency of 2.5 GHz. The respective errors compared to the simulated first resonant frequency when unloaded were 1.12% and 0.32%, which might have been caused by errors in fabrication and measurement. For the conventional patch antenna, the first resonant frequency of S_{11} moved from 2.498 GHz for the TLY-5A to 2.383 GHz for the RF-10, while it moved from 2.385 GHz for the TLY-5A to 1.938 GHz for the RF-10 in the proposed patch antenna. Table 4 summarizes these results.

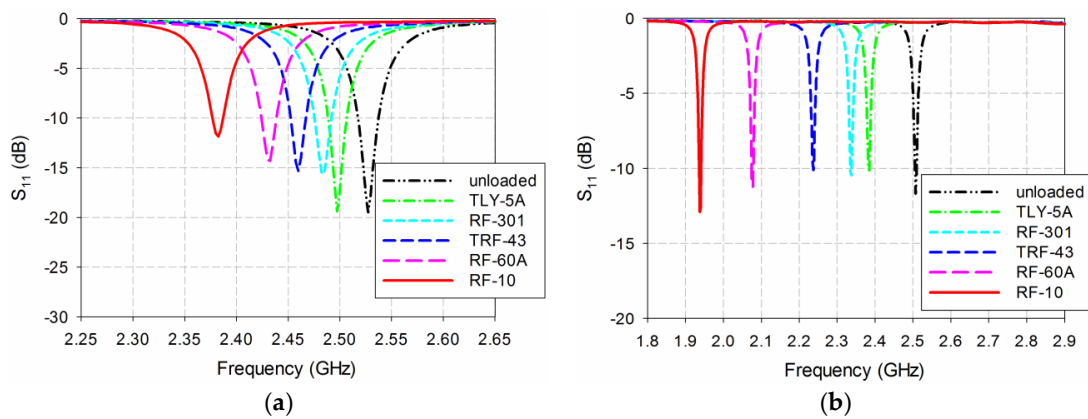


Figure 13. Measured S_{11} characteristics of the conventional and proposed patch antennas for the MUTs in Table 2: (a) Conventional; (b) proposed.

Table 4. Measured first resonant frequencies of S_{11} responses for the conventional and proposed patch antennas in GHz.

Antenna Type	Resonant Frequency	Unloaded ($\epsilon_r = 1$)	TLY-5A ($\epsilon_r = 2.17$)	RF-301 ($\epsilon_r = 2.97$)	TRF-43 ($\epsilon_r = 4.3$)	RF-60A ($\epsilon_r = 6.15$)	RF-10 ($\epsilon_r = 10.2$)
Conventional	f_{r1}	2.528	2.498	2.480	2.460	2.433	2.383
Proposed	f_{r1}	2.508	2.385	2.338	2.238	2.078	1.938

The measured sensitivities for the first resonant frequencies of the conventional and proposed patch antennas are compared in Figure 14. When TLY-5A ($\epsilon_r = 2.17$), RF-301 ($\epsilon_r = 2.97$), TRF-43 ($\epsilon_r = 4.3$), RF-60A ($\epsilon_r = 6.15$), and RF-10 ($\epsilon_r = 10.2$) were used as the MUT, in turn, the first resonant frequency shifts, Δf_r , of the conventional patch antennas were 0.030 GHz, 0.048 GHz, 0.068 GHz, 0.095 GHz, and 0.145 GHz, respectively, whereas those of the proposed patch antenna were 0.123 GHz, 0.170 GHz, 0.270 GHz, 0.430 GHz, and 0.570 GHz, respectively. The PRFS for the conventional patch antennas were 1.19%, 1.90%, 2.69%, 3.76%, and 5.74%, respectively, whereas the proposed patch antenna showed 4.90%, 6.78%, 10.77%, 17.15% and 22.73%, respectively. The PRFSE values for the first resonant frequency of the proposed patch antenna were 4.12, 3.57, 4.00, 4.56 and 3.96, respectively. The S values in the conventional patch antennas were 0.026 GHz, 0.024 GHz, 0.021 GHz, 0.018 GHz, and 0.016 GHz, respectively, whereas those in the proposed patch antenna were 0.105 GHz, 0.086 GHz, 0.082 GHz, 0.083 GHz, and 0.062 GHz, respectively. The SE values in the proposed patch antenna were 4.11, 3.54, 3.97, 4.53 and 3.92, respectively. Hence, the measured sensitivity of the proposed patch antenna was 3.54–4.53 times higher than the conventional patch antenna for the five MUTs, with relative permittivity ranging from 2.17 to 10.2, which was a slight increase, compared to the simulated results, due to fabrication and measurement errors.

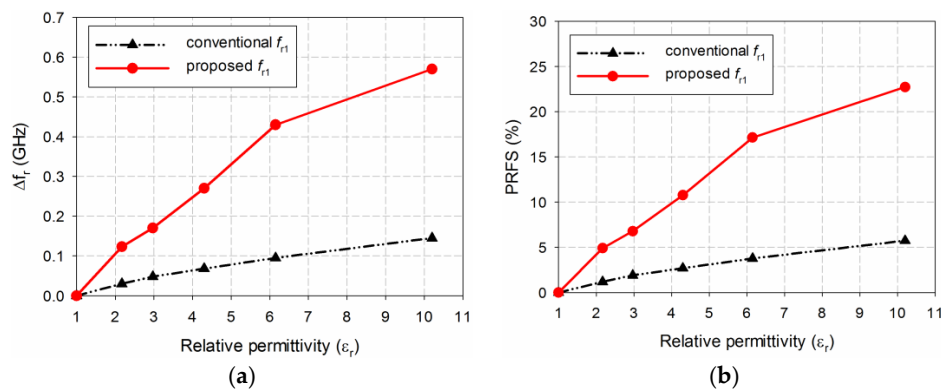


Figure 14. Cont.

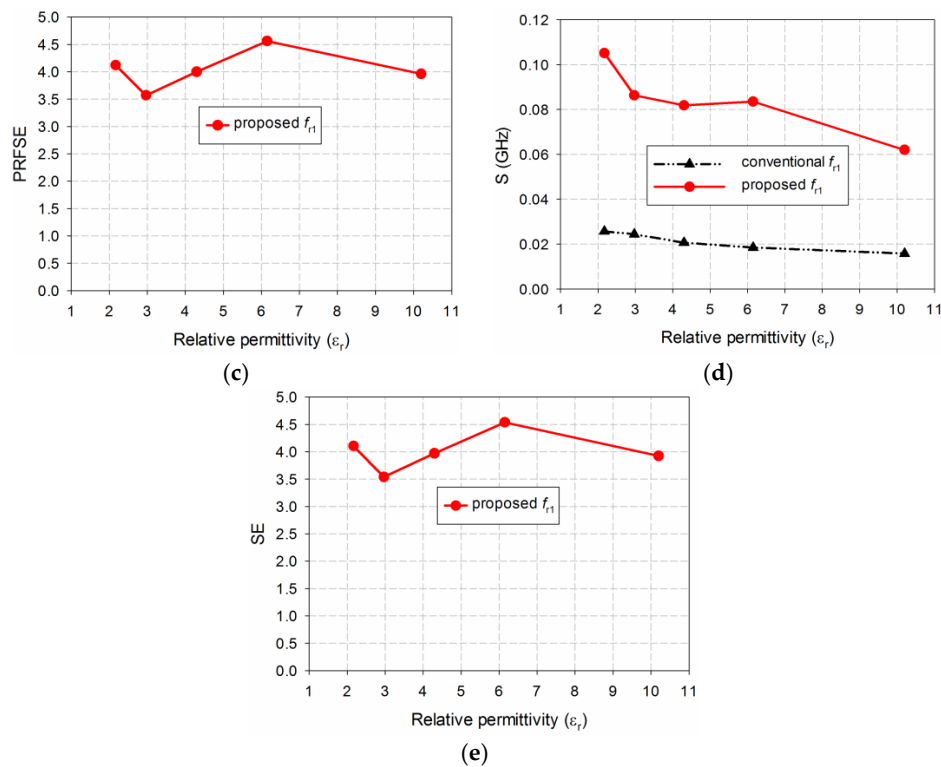


Figure 14. Measured sensitivity comparison of the conventional and proposed patch antennas for the MUTs in Table 2: (a) Δf_r ; (b) PRFS; (c) PRFSE; (d) S; (e) SE.

The differences in measured and simulated PRFS for the low permittivity MUT of the TLY-5A MUT were low at 0.21% to 0.34%, but the differences increased to 1.78% to 3.19% for the RF-10, which had high permittivity. In order to study the reasons for the differences in measured and simulated PRFS and the increasing error in the PRFS for the high permittivity MUT (RF-10), the simulated S_{11} characteristics of the conventional and proposed patch antennas were compared when the air gap between the MUT and the patch increased from 0 to 2 mm. For simulation, 18 different cases of the air gap were considered; 0, 0.005, 0.01, 0.02, 0.05, 0.1, 0.15, 0.2, 0.3, 0.4, 0.5, 0.6, 0.7, 0.8, 0.9, 1.0, 1.5, 2.0 (units in millimeter). First, the variations on the resonant frequency of the conventional patch antenna for 18 cases of varying the air gap are plotted in Figure 15a. The PRFS of the resonant frequency of the conventional patch antenna is shown in Figure 16a. When the air gap increased from 0 mm to 2 mm, the shift in the resonant frequency moved toward the high frequency with a nonlinear behavior. Note that the slope of the resonant frequency shift was higher for small air gap less than 0.2 mm and the amount of the frequency shift increased as the relative permittivity of the MUT increased. For instance, when TLY-5A was used as the MUT, PRFS of the conventional patch antenna was 0.30% for the air gap of 0.1 mm, whereas it was increased to 2.81% when RF-10 MUT was used.

For the proposed patch antenna, the variations on the resonant frequency for 18 cases of varying the air gap are plotted in Figure 15b and the PRFS of the resonant frequency is shown in Figure 16b. We observe that the trend of the resonant frequency shift was similar to the conventional patch antenna, but the amount was relatively large, which means more sensitive to the air gap. For example, when TLY-5A was used as the MUT, the PRFS of the proposed patch antenna was 2.03% for the air gap of 0.1 mm, whereas it was increased to 17.17% when RF-10 MUT was used. Therefore, the increasing error in the PRFS for the high permittivity MUT was observed by the simulation of the air gap between the MUT and the patch. In addition, the proposed patch antenna sensor was more sensitive to the air gap variation compared to the conventional patch antenna. In fact, plastic clips were used to fasten the MUT to the patch antenna, but it seems like that the pressure between the MUT and the antenna was not enough to guarantee perfect contact between the MUT and the antenna. Hence, imperfect contact

or a small air gap between the MUT and the antenna sensor made the error between the simulated and measured results. We will try to develop an accurate air gap control fixture or system for future work. The proposed slot-loaded patch antenna sensor can also be used for proximity detection applications by using the air gap variation.

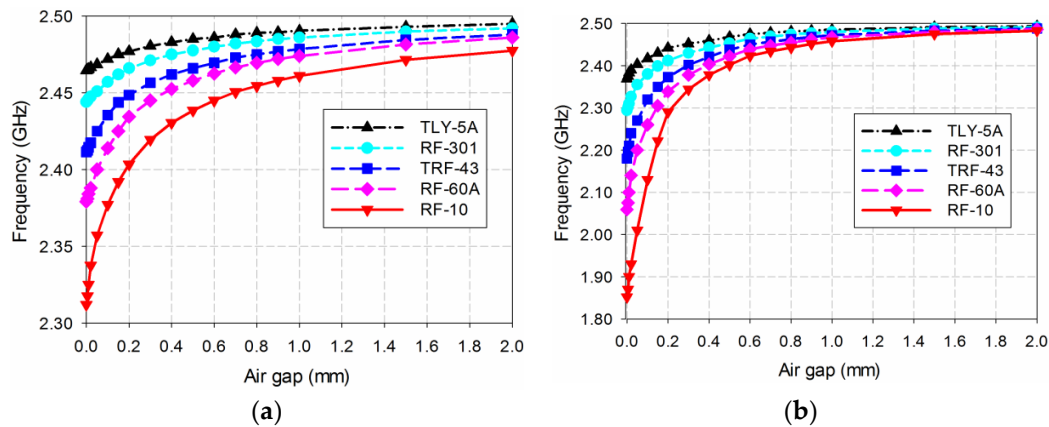


Figure 15. Variations on the resonant frequency of the conventional and proposed patch antennas when varying the air gap: (a) Conventional f_{r1} ; (b) proposed f_{r1} .

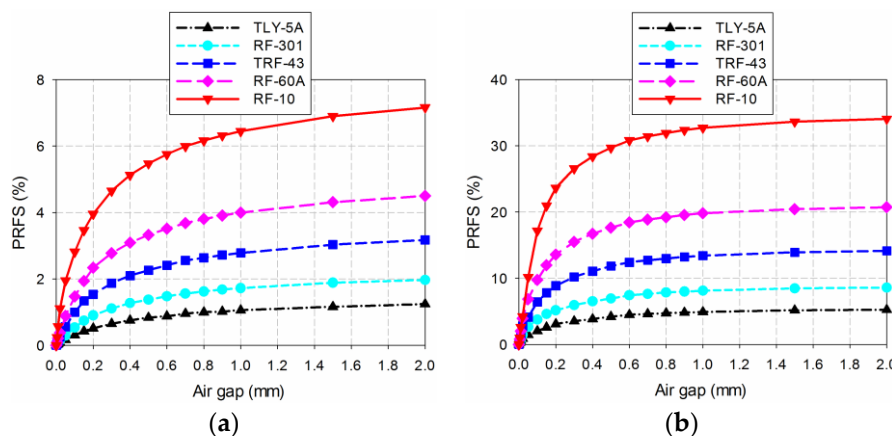


Figure 16. The PRFS of the resonant frequency of the conventional and proposed patch antennas when varying the length of the MUT: (a) Conventional f_{r1} ; (b) proposed f_{r1} .

5. Conclusions

A method of designing a high-sensitivity microstrip patch sensor antenna based on a thin rectangular slot loaded along the radiation edge of the patch for permittivity measurement at 2.5 GHz has been proposed. The sensitivity of the proposed slot-loaded patch antenna was compared with that of a conventional patch antenna without the slot by measuring the shift in the resonant frequency of the input reflection coefficient when five MUT superstrates were placed above the patch. The measured sensitivity of the proposed patch antenna is 3.54–4.53 times higher than the conventional patch antenna for the five MUTs with a relative permittivity ranging from 2.17 to 10.2. The effects of covering the feed line with the MUT and making an air gap between the MUT and the patch on the resonant frequency shift of the conventional and proposed patch antennas were also investigated.

The proposed high-sensitivity microstrip patch sensor antenna is expected to be used for permittivity characterization of planar solid and microfluidic liquid materials, for proximity detection in automation applications, for non-invasive determination of moisture content in soil, food or liquids, and for wireless sensing of biological samples or poisonous chemicals. Another possible application

would be for a simultaneous communication-and-sensing unit for chip-less RFID sensor tags measuring temperature, humidity, and other characteristics, and communicating with a reader, at the same time.

Author Contributions: J.Y. contributed the idea, simulation, analysis, and the overall research. J.-I.L. contributed fabrications and measurements.

Acknowledgments: This research was supported by Basic Science Research Program through the National Research Foundation of Korea (NRF) funded by the Ministry of Education (2018R1D1A1B07046040).

Conflicts of Interest: The authors declare no conflict of interest.

References

1. Saeed, K.; Shafique, M.F.; Byrne, M.B.; Hunter, I.C. Planar microwave sensors for complex permittivity characterization of materials and their applications. In *Applied Measurement System*; Haq, M.Z., Ed.; Intech: Rijeka, Croatia, 2012.
2. Fratticcioli, E.; Dionigi, M.; Sorrentino, R. A simple and low-cost measurement system for the complex permittivity characterization of materials. *IEEE Trans. Instrum. Meas.* **2004**, *53*, 1071–1077. [[CrossRef](#)]
3. Boybay, M.S.; Ramahi, O.M. Material characterization using complementary split-ring resonators. *IEEE Trans. Instrum. Meas.* **2012**, *61*, 3039–3046. [[CrossRef](#)]
4. Withayachumnankul, W.; Jaruwongrungrsee, K.; Adisorn, T.; Fumeaux, C.; Abbott, D. Metamaterial-based microfluidic sensor for dielectric characterization. *Sens. Actuators A-Phys.* **2013**, *189*, 233–237. [[CrossRef](#)]
5. Bernard, P.; Gautray, J. Measurement of dielectric constant using a microstrip ring resonator. *IEEE Trans. Microw. Theory Technol.* **1991**, *39*, 592–595. [[CrossRef](#)]
6. Saeed, K.; Guyette, A.; Pollard, R.; Hunter, I. Microstrip resonator technique for measuring dielectric permittivity of liquid solvents and for solution sensing. *Proc. IEEE MTT-S Int. Microw. Symp.* **2007**, 1185–1188.
7. Muhammed Shafi, K.T.; Ansari, M.A.H.; Jha, A.K.; Akhtar, M.J. Design of SRR-based microwave sensor for characterization of magnetodielectric substrates. *IEEE Microw. Wirel. Compon. Lett.* **2017**, *27*, 524–526.
8. Velez, P.; Su, L.; Grenier, K.; Mata-Contreras, J.; Dubuc, D.; Martin, F. Microwave microfluidic sensor based on a microstrip splitter/combiner configuration and split ring Resonators (SRRs) for dielectric characterization of liquids. *IEEE Sens. J.* **2017**, *17*, 6589–6598. [[CrossRef](#)]
9. Ebrahimi, A.; Scott, J.; Ghorbani, K. Differential sensors using microstrip lines loaded with two split ring resonators. *IEEE Sens. J.* **2018**, *18*, 5786–5793. [[CrossRef](#)]
10. Lee, C.S.; Yang, C.L. Thickness and permittivity measurement in multi-layered dielectric structures using complementary split-ring resonators. *IEEE Sens. J.* **2014**, *14*, 695–700. [[CrossRef](#)]
11. Lee, C.S.; Yang, C.L. Complementary split-ring resonators for measuring dielectric constants and loss tangents. *IEEE Microw. Wirel. Compon. Lett.* **2014**, *24*, 563–565. [[CrossRef](#)]
12. Ebrahimi, A.; Withayachumnankul, W.; Al-Sarawi, S.; Abbott, D. High-sensitivity metamaterial-inspired sensor for microfluidic dielectric characterization. *IEEE Sens. J.* **2014**, *14*, 1345–1351. [[CrossRef](#)]
13. Ansari, M.A.H.; Jha, A.K.; Akhtar, M.J. Design and application of the CSRR-based planar sensor for noninvasive measurement of complex permittivity. *IEEE Sens. J.* **2015**, *15*, 7181–7189. [[CrossRef](#)]
14. Yang, C.L.; Lee, C.S.; Chen, K.W.; Chen, K.Z. Noncontact measurement of complex permittivity and thickness by using planar resonators. *IEEE Trans. Microw. Theory Technol.* **2016**, *64*, 247–257. [[CrossRef](#)]
15. Su, L.; Mata-Contreras, J.; Naqui, J.; Martín, F. Splitter/combiner microstrip sections loaded with pairs of complementary split ring resonators (CSRRs): Modeling and optimization for differential sensing applications. *IEEE Trans. Microw. Theory Technol.* **2016**, *64*, 4362–4370. [[CrossRef](#)]
16. Su, L.; Mata-Contreras, J.; Vélez, P.; Fernández-Prieto, A. Analytical method to estimate the complex permittivity of oil samples. *Sensors* **2018**, *18*, 984. [[CrossRef](#)]
17. Ansari, M.A.H.; Jha, A.K.; Akhter, Z.; Akhtar, M.J. Multi-band RF planar sensor using complementary split ring resonator for testing of dielectric materials. *IEEE Sens. J.* **2018**, *18*, 6596–6606. [[CrossRef](#)]
18. Li, C.; Li, F. Characterization and modeling of a microstrip line loaded with complementary split-ring resonators (CSRRs) and its application to highpass filters. *J. Phys. D Appl. Phys.* **2007**, *40*, 3780–3787. [[CrossRef](#)]

19. Sha, K.T.M.; Jha, A.K.; Akhtar, M.J. Improved planar resonant RF sensor for retrieval of permittivity and permeability of materials. *IEEE Sens. J.* **2017**, *17*, 5479–5486.
20. Yeo, J.; Lee, J.-I. High-sensitivity microwave sensor based on an interdigital-capacitor-shaped defected ground structure for permittivity characterization. *Sensors* **2019**, *19*, 498. [[CrossRef](#)] [[PubMed](#)]
21. Bahl, I.J.; Bhartia, P.; Stuchly, S.S. Design of microstrip antennas covered with a dielectric layer. *IEEE Trans. Antennas Propag.* **1982**, *30*, 314–318. [[CrossRef](#)]
22. Zoughi, R.; Vaughan, T. Analysis of microstrip patch antennas for dielectric measurement. *Rev. Prog. Quant. Non-Destr. Eval.* **1990**, *9*, 521–528.
23. Bogosanovich, M. Microstrip patch antenna sensor for measurement of the permittivity of homogeneous dielectric materials. In Proceedings of the 16th IEEE Instrumentation and Measurement Technology Conference, Venice, Italy, 24–26 May 1999; pp. 31–36.
24. Bogosanovich, M. Microstrip patch sensor for measurement of the permittivity of homogeneous dielectric materials. *IEEE Trans. Instrum. Meas.* **2000**, *49*, 1144–1148. [[CrossRef](#)]
25. You, K.Y.; Salleh, J.; Abbas, Z.; You, L.L. A rectangular patch antenna technique for the determination of moisture content in soil. *PIERS Proc.* **2010**, 850–854.
26. Yahaya, N.Z.; Abbas, Z.; Ali, B.M.; Ismail, A.; Ansarudin, A.F. Intercomparison of methods for determination of resonant frequency shift of a microstrip patch antenna loaded with hevea rubber latex. *J. Sens.* **2014**, *2014*, 656972. [[CrossRef](#)]
27. Lee, K.; Hassan, A.; Lee, C.H.; Bae, J. Microstrip patch sensor for salinity determination. *Sensors* **2017**, *17*, 2941. [[CrossRef](#)]
28. Han, J.; Geyi, W. A new method for measuring the properties of dielectric materials. *IEEE Antennas Wirel. Propag. Lett.* **2013**, *12*, 425–428. [[CrossRef](#)]
29. Jiang, J.; Geyi, W. Development of a new prototype system for measuring the permittivity of dielectric materials. *J. Eng.* **2014**, *2014*, 302–304. [[CrossRef](#)]
30. Shahpari, M. Determination of complex conductivity of thin strips with a transmission method. *Electronics* **2019**, *8*, 21. [[CrossRef](#)]
31. Girbau, D.; Ramos, A.; Lazaro, A.; Rima, S.; Villarino, R. Passive wireless temperature sensor based on time-coded UWB chipless RFID tags. *IEEE Trans. Microw. Theory Technol.* **2012**, *60*, 3623–3632. [[CrossRef](#)]
32. Cheng, H.; Ebadi, S.; Gong, X. A low-profile wireless passive temperature sensor using resonator/antenna integration up to 1000 °C. *IEEE Antennas Wirel. Propag. Lett.* **2012**, *11*, 369–372.
33. Yao, J.; Tjuatja, S.; Huang, H. Real-time vibratory strain sensing using passive wireless antenna sensor. *IEEE Sens. J.* **2015**, *15*, 4338–4345. [[CrossRef](#)]
34. Yao, J.; Tchafa, F.M.; Jain, A.; Tjuatja, S.; Huang, H. Far-field interrogation of microstrip patch antenna for temperature sensing without electronics. *IEEE Sens. J.* **2016**, *16*, 7053–7060. [[CrossRef](#)]
35. Huang, Y.; Boyle, K. *Antennas: From Theory to Practice*; John Wiley & Sons: Hoboken, NJ, USA, 2008.
36. Maci, S.; Biffi Gentili, G.; Piazzesi, P.; Salvador, C. Dual-band slot-loaded patch antenna. *Microw. Antennas Propag.* **1995**, *142*, 225–232. [[CrossRef](#)]
37. Salim, A.; Lim, S. Complementary split-ring resonator-loaded microfluidic ethanol chemical sensor. *Sensors* **2016**, *16*, 1802. [[CrossRef](#)] [[PubMed](#)]
38. Taconic PTFE Laminates. Available online: http://www.taconic.co.kr/pages/sub02_03.php (accessed on 2 April 2019).

